The Influence of Dipole Spindown and Mass Fallback on Magnetars as Central Engines for Long Gamma Ray Bursts

David Vartanyan

Senior Thesis
Astrophysics Program
California Institute of Technology

Abstract

We explore the viability of magnetars associated with core-collapse supernovae (SNe) as central engines of long gamma-ray bursts (LGBRs). Magnetars are rapidly spinning neutron stars with strong magnetic fields. Magnetars with fields of $\sim 10^{15} - 10^{16}$ G, a range of initial masses $1.4 - 2.5\,M_\odot$, and formation periods of ~ 1 ms have sufficient rotational energy to power LGRBs. Furthermore, magnetar formation associated with Type Ibc SNe is consistent with the fraction of SNe Ibc SNe associated with LGRBs. We study the robustness of magnetars in powering both prompt emission and afterglow features in LGRB lightcurves in the context of magnetar spindown and mass accretion. In doing so, we address fallback accretion and the possibility of a magnetar propelling infalling material outward. We find that if a magnetar is in the propeller regime in the first $100\,\mathrm{s}$, it will spindown by several milliseconds but extend the duration of prompt emission and prevent early accretion-induced collapse to a black hole. Furthermore, we explore an afterglow powered by dipole spindown and coupled with fallback, either in the accretion or propeller regime. We find that, for certain initial periods, magnetar mass and accretion rates, and magnetic fields, a magnetar may power a lightcurve plateau up to over $1000\,\mathrm{s}$.

Contents

1   Introduction

Gamma-ray bursts were first discovered during the Cold War. The United States launched the VELA, Spanish for *watchman*, satellite system in 1963 to monitor SALT treaty bans on atomic bomb testing. In 1967, the satellites detected a flash of gamma rays. The isotropic distribution of these so called gamma ray bursts (GRBs) provided early evidence that GRBs originated outside the Milky Way. Otherwise, we would expect a distribution along the galactic plane. However, the first accurate distance determination of a GRB was not performed until 1997, when Mark Metzger analyzed GRB 970508 to have a redshift $z = 0.835$, providing further evidence that GRBs occur in distant galaxies. Today, a GRB is detected every couple of days with the advent of SWIFT. Due to their high redshift and energies, GRBs provide the opportunity to explore deep space cosmology, early star formation in association with supernova, and high-energy nuclear physics. Ironically, with SWIFT superceding BATSE in 2004, the rampant discovery of GRBs has prevented systematic calculation of GRB redshifts.

GRBs are categorized by their duration and hardness. The duration is characterized by a T_{90} value, defined as the interval during which 90% of the photon count of a GRB is detected. Long gamma ray-bursts (LGRBs) have T_{90} values peaking at $30 - 60$ seconds, though many have been detected with T_{90} over 100 seconds. By comparison, short gamma-ray bursts (SGRBs) have T_{90} ranging between $0.3 - 2$ seconds (see NASA's documentation [1], Kouvelitou et al. 1993 [2] and Qin et al. 2013 [3]). Categorically, SGRBs have harder spectra, containing a larger fraction of high-energy photons, whereas LGRBs have softer spectra. SGRBs also typically have lower energies than LGRBs [4]. LGRBs and SGRBs are assumed to have different central engines. For a review on SGRBs, extended emission in SGRBs, and evidence for a magnetar as a central engine in SGRBs, see Nakamura et al. 2013 [5], Gompertz et al. 2013 [6], and Rowlinson et al. 2010 [7]. In this paper, we will focus on LGRBs.

A GRB jet is thought to be driven by either a fireball model [8] or a Poynting flux model [9]. GRB lightcurves feature a prompt emission phase with T_{90} values described above and an afterglow phase in some cases lasting over 1000 seconds. The prescribed model must explain these features as well as account for nonthermal emission. The fireball model involves a central engine that deposits a large amount of energy, of order 10^{51} ergs, inside a diameter of $\sim 100\,\mathrm{km}$ with low baryon density. The baryon density is sufficient to trap the photons, converting the deposited energy into kinetic energy. The fireball thus accelerates the baryons to ultrarelativistic velocities. A quick calculation can constrain the baryonic mass. To reach a Lorentz factor of $\Gamma \approx E/Mc^2$, the baryonic mass M_b must be less than

$$M_b = \frac{E}{\Gamma c^2} \approx 6 \times 10^{-6} M_\odot \left(\frac{E}{10^{51}\mathrm{ergs}}\right)\left(\frac{100}{\Gamma}\right). \tag{1}$$

The Poynting flux-driven jet similarly involves a large injection of energy within a similarly small radius. However, the Poynting flux model is characterized by large-scale magnetic fields, and baryons and baryon acceleration play little role. Internal shocks, magnetic dissipation, or a combination of both are thought to produce the prompt gamma ray emission (see Sec. 3.2). A Poynting flux driven jet favors a magnetic dissipation model rather than shocks to power the prompt emission (see Metzger et al. 2010 [9] and Woosley et al. 2006 [10]). Magnetic dissipation accelerates and heats electrons to temperatures conducive to Inverse-Compton scattering which forms the bulk of the prompt emission radiation [9]. In the case of shocks, ultrarelativistic baryons interact via collisionless shocks, mediated by electric and magnetic fields rather than particle interactions, resulting in synchrotron radiation powering the prompt emission light curve instead of Inverse-Compton scattering[9].

In either case, inverse Compton and synchtron radiation produce the nonthermal prompt emission feature. External shocks are thought to produce the afterglow. The outflow decelerates and interacts with either the ISM or a wind ejected earlier to produce a lightcurve afterglow in the X-ray to the radio bands (see Meszaros 2006 [11]).

1.1   LGRB-SN Connection

Paczyński 1986 [12] first suggested that the kinetic energy of core-collapse supernovae corresponded to the energy released in LGRBs. Early measurements of LGRB redshifts implied energies of 10^{54} ergs assuming isotropic emission, a factor of 1000 greater than expected and in some cases greater than the

rest mass of the NS. The isotropic assumption for GRBs was quickly droped since beaming corrections would return expected energies of 10^{51} ergs. Early observational evidence for a LGRB-SN connection was provided by localization of LGRBs in distant, actively star-forming galaxies [10][13]. Subsequent detection of SN 1c-bl fingerprints in late time afterglows of LGRB lightcurves provided more direct proof for the SN-GRB connection [14]. Detection of SN 1998bw 2.5 days after GRB 980425 provided the first LGRB-SN association [15].

Type Ibc-bl, broad-lined core-collapse SNe associated with GRBs form a small fraction of all supernovae (see Hjorth & Bloom 2011 [16] and Bernardini et al. 2013 [17]). Magnetars comprise $\sim 10\%$ of neutron star births, and Gaensler et al. 2005 [18] expect a similar fraction of SNe Ibc to result in magnetars. Not all magnetars, however, will have sufficient magnetic fields and spin periods to power LGRBs. Estimates (see Guetta & Della Valle 2006 [19]) constrain $\sim 1 - 9\%$ of SNe Ibc-bl to be associated with low-luminosity GRBs and $\sim 0.3 - 3\%$ with normal LGRBs, while radio observations by Soderberg et al. 2010b [20] independently constrain $< 1\%$ of SNe-bc of SNe Ibc to harbour central engines. Uncertainty in the LGRB jet beaming angle account for the uncertainty in the LGRB population in SNe Ibc. Given uncertainties in the SN Ibc-bl rate among all SN Ibc, Modjaz 2011 [14] argues that the LGRB rate in SN Ibc-bl is broadly consistent with the expected fraction of SNe to harbor central engines.

1.2 Magnetar Model

One possibility for the central engine of LGRBs is a magnetar, a rapidly rotating and highly magnetized neutron star (NS). Magnetars are hypothesized to extract rotational energy to power strong magnetic fields and drive a GRB powered by either a Poynting flux and/or a magnetized wind. During the collapse of the progenitor, according to the 'toothpaste model,'[21] [22] the infalling envelope is thought to confine and collimate the central engine outflow into a jet (see Uzdensky & MacFadyen 2007 [21]). A magnetar, with an initial period at the beginning of prompt emission of 1 ms and magnetic fields on the order of $B \approx 10^{15}$ G will have a rotational energy $E \approx I\Omega^2/2 \approx 10^{52}$ ergs and an initial dipole spindown luminosity of $L \approx B^2 R^6 \Omega^4/c^3 \approx 10^{50}$ erg s^{-1}, typical of GRBs and associated SNe [10]. At radii $\sim 10^{16}$ cm, the magnetar energy outflow is hypothesized to accelerate and thermalize the baryon or lepton content surrounding the magnetar (see Sec. 3.2). Depending on the emission model, either magnetic dissipation or internal shocks power the prompt emission phase of the LGRB. At times > 100 s the dipole spindown is thought to dominate the magnetar's radiation and power the afterglow. The various stages of the magnetar's period evolution are explored in Sec. 3 and Sec. 4.

1.3 Collapsar Model

Another possibility for an LGRB central engine is the collapsar model (see Woosley 1993 [23]). The collapsar model involves a black hole (BH) forming inside a massive star with sufficient specific angular momentum to form a disk. Accretion onto the black hole is thought to power the LGRB. For a nonrotating black hole, the specific angular momentum j required is $j = 2\sqrt{3}GM/c \approx 4.6 \times 10^{16} M_{\rm bh}/3$ cm^2 s^{-1} [10]. For a maximally rotating (Kerr) black hole, the required specific angular momentum is $j = 2/\sqrt{3}GM/c \approx 1.5 \times 10^{16} M_{\rm bh}$ cm^2 s^{-1} [10], where $M_{\rm bh}$ is the black hole mass in solar masses. By comparison, the requisite angular momentum to form a magnetar with initial period at prompt emission of 1 ms and a radius of 12 km is $R^2\Omega \approx 9 \times 10^{15}$ cm^2 s, slightly less than that for a nonrotating black hole.

Dessart et al. 2012 suggest that magnetars, however, are more easily produced by current stellar models [24]. They argue that black hole formation is non-trivial since only the fastest rotating progenitors reach the core compactness necessary for black hole formation [24]. Furthermore, the majority of sufficiently compact progenitors retain enough angular momentum to leave them prone to magnetorotational instability that prefers magnetar formation [24]. Furthermore, the progenitor metallicity and envelope mass are not compatible with LGRB observations. Woosley & Heger 2006 [25] constrain LGRB progenitors to lower mass stars, reducing candidates for BH formation, based on detected LGRB/SNe ejecta masses of $\sim 10 M_{\odot}$ and the assumption that higher-mass stars lose too much angular momentum through metallicity-driven stellar winds.

The remainder of the paper is organized as follows. In Sec. 2, we discuss dipole spindown of a magnetar as a central engine for LGRBs. We introduce the concept of magnetization and explain how we will adjust the spindown model to account for possible mass fallback. In Sec. 3, we study in more detail the period evolution of a magnetar during its prompt emission phase, including the effects of a propeller regime. In Sec. 4, we study the period evolution of a magnetar during the afterglow phase and search for possible models that allow a lengthy plateau. We account for fallback accretion and inundate the reader with plots. Finally, in Sec. 5, we summarize our results in the context of existing work and discuss future possibilities.

2   Magnetar Spindown as a Source of LGRB Engine Power

We explore the fundamental physics of magnetar spindown as it relates to both the prompt emission and the afterglow phases of the LGRB light curve. In Section 2.1, we introduce the magnetization parameter σ, relevant for our subsequent discussion of the prompt emission energetics and duration. In Section 2.2, we will then derive the dipole model for magnetar spindown, which will be relevant for our discussion of afterglow plateaus. Finally, in Section 2.3, we will follow Piro & Ott 2011 [26] to account for possible fallback accretion onto our magnetar. This may affect both prompt emission and afterglow energetics and duration by modifying the magnetization parameter and the magnetar period. We are particularly interested in the possibility of accretion-induced collapse to a black hole, thus shutting off the magnetar engine and ending the plateau.

2.1   Magnetization

The magnetization parameter is defined as

$$\sigma_o = \frac{\phi^2 \Omega^2}{\dot{M} c^3} \ , \tag{2}$$

where ϕ is the poloidal magnetic flux, Ω is the angular frequency, and $\dot{M}$ is the mass loss rate. Naively, we can think of magnetization as a ratio of magnetic field energy density to mass energy density. As will be discussed in Section 3, the magnetization parameter increases drastically on a timescale of $20 - 100\,\mathrm{s}$, during which the neutron star becomes optically thin to neutrinos and consequently the neutrino-driven mass loss, $\dot{M}$, declines [9]. Neutrino driven mass loss results from neutrino heating in the NS atmosphere following the reactions:

$$\begin{cases} \nu_e + n \leftrightarrow e^- + p \\ \overline{\nu}_e + p \leftrightarrow e^+ + n \,. \end{cases} \tag{3}$$

From Qian & Woosley 1996 [27], the mass loss for unmagnetized winds can be approximated by,

$$\dot{M}_\nu = 5 \times 10^{-5}\,\mathrm{M_\odot\,s^{-1}} \left(\frac{L_\nu}{10^{52}\,\mathrm{ergs\,s^{-1}}} \right) \times \left(\frac{\epsilon_\nu}{10\,\mathrm{MeV}} \right)^{10/3} \left(\frac{M}{1.4\,\mathrm{M_\odot}} \right)^{-2} \left(\frac{R}{10\,\mathrm{km}} \right)^{5/3} (1 + \epsilon_{es})^{5/3} . \tag{4}$$

ϵ_ν is the mean neutrino energy, ϵ_{es} is a correction for heating due to inelastic electron scattering. Metzger et al. 2010 [9] additionally correct for a strong magnetic field and rapid rotation. The key point, however, is the scaling with the neutrino luminosity, L_ν. The neutrino diffusion timescale constrains the prompt emission duration since jets with high magnetization cannot effectively accelerate and dissipate their energy [9]. Instead, most of the available rotational energy of the neutron star would remain as a Poynting flux rather than thermalizing to produce emission [9]. Observational knowledge of neutrino diffusion times is limited. For reference, SN 1987A had a diffusion of timescale of $\sim 10\,\mathrm{s}$, whereas the duration of typical LGRBs is $\sim 100\,\mathrm{s}$, and typical neutrino diffusion times for neutron stars are few tens of seconds from Cacciapaglia 2002 [28]. Metzger et al. 2010 [9] cite $20 - 100\,\mathrm{s}$ for the neutrino diffusion timescale. This generous upper limit is a stiff function of opacity and highly sensitive to the interior temperature of the neutron star. Metzger et al. 2010 [9] allow for a factor of 3 increase in L_ν to account for rapid rotation of the NS, which decreases interior temperature of the NS and thus slows its cooling

evolution. This, however, constrains the upper limitof prompt emission duration to $30-60\,\mathrm{s}$. justify an upper limit of $100\,\mathrm{s}$, we search for additional physical processes that may decrease the magnetization in order to prolong the prompt emission duration to $\sim 100\,\mathrm{s}$, a duration typical of prompt emissions of observed LGRBs. Barring decreasing the magnetix flux or the angular frequency, which would also counterproductively decrease the spindown energy, or increasing the speed of light, which stubbornly chooses to remain constant, we are left with increasing $\dot{M}$.

2.2 Magnetar Dipole Radiation

We model magnetar spindown similarly to pulsars and assume a magnetic dipole toy model [8]. The dipolar magnetar field is:

$$B(\vec{r}) = \frac{3\vec{n}(\vec{m}.\vec{n}) - \vec{m}}{r^3}, \tag{5}$$

where $\vec{m}$ is the magnetic moment and $\vec{n}$ is the unit radial vector.

In analogy with Larmor's formula for electric dipole radiation, a time-dependent magnetic dipole radiates

$$\frac{dW}{dt} = -\frac{2}{3c^3}|\dddot{\vec{m}}_\perp|^2, \tag{6}$$

where $\vec{m}_\perp$ is the component of $\vec{m}$ perpendicular to the rotation axis.

Defining the angle between the rotation axis and the magnetic dipole moment as α,

$$\vec{m}_\perp = m_o \sin(\alpha)e^{-i\Omega t}, \tag{7}$$

so $|\dddot{\vec{m}}|_\perp^2 = m_o{}^2 \sin \alpha^2 \Omega^4$ since $m_o = BR^3/2$ for a uniformly magnetized sphere.

It follows that the time-averaged dipole radiation is

$$\frac{dW}{dt} = -\frac{B_p{}^2 R^6}{6c^3}\Omega^4 \sin^2 \alpha \,. \tag{8}$$

The larger the angular separation α of the magnetic and rotational axes is, the greater the dipole radiation will be. For simplicity, we assume the magnetic dipole is oriented perpendicularly to the rotation axis so $\alpha = \pi/2$. We define the magnetar spin period $P = 2\pi/\Omega$ and arrive at Eq. 2 from Lyons et al. 2009 [29],

$$L = 9.62065 \times 10^{48}\, B_{p,15}^2 P_{-3}^{-4} R_6^6 \,\mathrm{erg\,s}^{-1}, \tag{9}$$

where $B_{p,15} = B_p/10^{15}\,\mathrm{G}$, $P_{-3} = P/10^3\,\mathrm{s}$, and $R_6 = R/10^6\,\mathrm{km}$.

Next we assume dipole radiation taps the rotational energy of the magnetar, so $\frac{dE_{rot}}{dt} = \frac{dW}{dt}$ where $E_{rot} = 1/2\,Iw^2$ so $\dot{E}_{rot} = I\omega\dot{\omega}$. Define a characteristic dipole spindown time τ_{dipole} as $\tau_{\mathrm{dipole}} = -\omega/\dot{\omega}$. It follows that

$$\tau_{\mathrm{dipole}} = \frac{3c^3 I}{B_p{}^2 R^6 \omega^6} \,, \tag{10}$$

Then,

$$\tau_{\mathrm{dipole}} = 2051.75\ I_{45} B_{15,p}^{-2} P_{-3}^2 R_6^{-6}\,\mathrm{s} \,, \tag{11}$$

which is Eq. 3 in Lyons et al. 2009 [29]. $I_{45} = I/10^{45}\,\mathrm{g\,cm}^2$. We allow for some oblateness, so $I = 0.35MR^2$ following Lattimer & Prakash 2001 [30]. We will refer to the above derivation as the classical derivation for magnetar dipole radiation. Lyons et al. assume $P = P_o$, using the initial period at the beginning of prompt emission and neglecting spindown.

While the classical derivation of a magnetic dipole yields no luminosity when the spin and magnetic axes are aligned, Spitkovksy 2008 [31] derives the time-dependent radiation for a force-free pulsar with a magnetosphere dominated by inertia-free plasma,

$$L_{\text{pulsar}} = k_1 \frac{\mu^2 \Omega^4}{c^3} (1 + k_2 \sin^2 a) \ , \tag{12}$$

where the cofactors are nearly unity, $k_1 = 1 \pm 0.05$, $k_2 = 1 \pm .01$. The key difference between Spitkovsky's model and the classical derivation above is that the former not only allows for a magnetar to produce dipole radiation even if its magnetic and rotational axes are aligned, but also allows for a higher spindown powered luminosity. For maximally misaligned, or orthogonal, axes, Spitkovsky's force-free model allows for magnetar radiation up to twice the classically-derived spindown model. And even when aligned, Spitkovsky's force-free magnetar produces dipole radiation roughly equal to classical magnetars with orthogonal axes. However, when we consider mass accretion, we will no longer be in the nearly force-free regime and this assumption will no longer be applicable. Unless stated otherwise, we follow Bucciantini et al. 2007 [22] in assuming the dipole axis is orthogonal to the rotation axis.

2.3 Fallback Accretion and the Propeller Mechanism

We are interested in solving for the magnetar period evolution in the presence of fallback accretion. Thus, we assume a supernova inefficiently stripping the stellar envelope, leaving the magnetar in a nonvacuum environment. We will follow Piro & Ott 2011 [26] in the following.

Accretion falls under the magnetar's field influence at the Alfvén radius,

$$r_m = \mu^{4/7} (GM)^{-1/7} \dot{M}^{-2/7}, \tag{13}$$

where μ is twice the magnetar moment, m_o, defined in Section 2.2. The Alfvén radius is derived by calculating the distance from the neutron star where the magnetic field energy density, $B^2/8\pi$, becomes comparable to the kinetic energy density of infalling matter, $1/2\rho v^2$, where ρ is the mass density of the accreting material and v its velocity. We assume that the accreting material is in radial free-fall, so the free-fall velocity $v_{\text{ff}} = \sqrt{2GM/r}$, where M is the neutron star mass and r the distance of the infalling material from the neutron star. Imposing the continuity equation of mass, $\rho = \dot{M}/(4\pi v_{\text{ff}} r^2)$. Equating these two, we obtain Eq. 13.

Material will corotate with the magnetar up to the corotation radius,

$$r_c = \left(\frac{GM}{\Omega^2} \right)^{1/3}, \tag{14}$$

derived from equating maximal accretion orbital velocity to the Keplerian velocity, $\Omega = \sqrt{GM/R^3}$ in the limit of orbiting material of negligible mass. M is the magnetar mass and R its equatorial radius.

If $r_m > r_c$, infalling material under the influence of the neutron star's dipole field must spin at a super-Keplerian rate to corotate with the neutron star and is thus flung out. If $r_m < r_c$, material will come under the dipole field's influence and corotate with the neutron star at the Keplerian velocity and subsequently be funneled onto the magnetar. This delineates the accretion regime from the propeller regime.

Then, we can solve for the magnetar period dynamics by conserving angular momentum

$$I \frac{d\Omega}{dt} = N_{dip} + N_{acc} \ , \tag{15}$$

where

$$N_{dip} = -\frac{\mu^2 \Omega^3}{6c^3}. \tag{16}$$

We divide N_{acc} into two cases: when $r_m > R$ and and when $r_m < R$. Only in the first case does infalling material come under the dipole field's influence.

We then have

$$N_{acc} = n(\omega)(GMr_m)^{1/2} \dot{M} \text{ for } r_m > R \ , \tag{17}$$

7

where $\omega = (\frac{\Omega}{GM/r_m^3})^{1/2} = (r_m/r_c)^{3/2}$. $n(\omega)$ must be fixed such that N_{acc} is positive, spinning up the magnetar, in the accretion regime $r_m < r_c$ and negative, spinning down the magnetar, in the propeller regime, $r_m > r_c$. Otherwise, if $r_m = r_c$, $n(\omega) = 0$. Following Piro and Ott 2011 [26], we set $n(\omega) = 1 - \omega$. For an Alfven radius internal to the magnetar, $r_m < R$, we have

$$N_{acc} = (1 - \frac{\Omega}{\Omega_k})(GMR)^{1/2}\dot{M} \text{ for } r_m < R. \tag{18}$$

Infalling material does not come under the influence of the magnetic field before accretion. The prefactor ensures continuity of N_{acc} at $r_m = R$.

The mass accretion rate can be decomposed into early and late times,

$$\dot{M}_{early} = \eta 10^{-3} t^{1/2} \, \text{M}_\odot \text{s}^{-1}, \tag{19}$$

$$\dot{M}_{late} = 50 t^{-5/3} \, \text{M}_\odot \text{s}^{-1}, \tag{20}$$

following Macfadyen et al. 2001 [32] and Zhang et al. 2008 [33]. $\eta \approx 0.1 - 10$ is a dimensionless parameter roughly indicating the efficiency of the supernova in removing the stellar envelope. A larger η signifies less efficient removal of the envelope and hence more fallback. Late-time accretion is roughly independent of η. Following the convention in Piro and Ott 2011, we combine these expressions

$$\dot{M} = (\dot{M}_{early}^{-1} + \dot{M}_{late}^{-1})^{-1}, \tag{21}$$

This has the virtue of returning Eq. 19 at early times and Eq. 20 at late times. Other conventions are possible, but for consistency we follow Piro & Ott 2011 [26].

Early in the magnetar's lightcurve, during the prompt emission phase, magnetar spindown is dominated by wind loss and possibly dipole spindown if the magnetar is in the propeller regime and thus losing angular momentum to the propelled outflow. If the magnetar transitions to an accreting regime before a few 100 s, we expect a dip in the magnetar period due to fallback accretion spinning up the magnetar. At late times, however, the dipole spindown will dominate. The different stages of a magnetar's period evolution are explored in the subsequent sections.

3   Prompt Emission and Magnetic Dissipation

Can accreting material being propelled outward increase $\dot{M}$ and hence lower magnetization to allow for longer prompt emission winds? Metzger et al. 2010 [9] solve for prompt emission energetics assuming neutrino-driven mass loss (an outflow). We cannot similarly account for accreting mass from the supernova (an inflow) in calculating the magnetization. Rather, following Piro & Ott 2011 [26], there exist certain conditions under which fallback accretion is flung back out. We will explore the effects of a magnetar in this propeller regime in the first 100 s to modify the magnetar's prompt emission period evolution calculated in Metzger et al. 2010 [9]. In Sec. 3.1, we explore the duration of prompt emission on magnetization and study the period evolution for different spindown models and allow for mass fallback. In Sec. 3.2, we compare magnetization dissipation vs internal shocks as the expected mechanism for prompt emission in magnetars.

3.1   Magnetization and Longevity

In order to produce the prompt emission of the LGRB, the jet must both accelerate to a high Lorentz factor and dissipate its energy internally. At the corotation radius of $\sim 10^7$ cm, the energy is primarily in a Poynting flux. However, by a radius of $\sim 10^{12} - 10^{17}$ cm, where prompt emission occurs, this energy must be converted into kinetic and possibly thermal energy. Metzger et al. 2010 [9] cite magnetic dissipation as the means of acceleration and possibly emission. Magnetic dissipation involves a breakdown of ideal

MHD. One possibility is the magnetic and spin axes are not aligned (see Lyubarsky & Kirk 2001 [34]. This non-axisymmetric geometry allows for magnetic reconnection up to the magnetic saturation radius,

$$R_{\mathrm{mag}} = \frac{\pi c \sigma^2}{3\epsilon\Omega} \approx 5 \times 10^{12} \, \mathrm{cm} \left(\frac{\sigma}{10^2}\right) \left(\frac{P}{\mathrm{ms}}\right) \left(\frac{\epsilon}{0.01}\right)^{-1} \, , \tag{22}$$

where σ is the magnetization, Ω is the magnetar angular frequency, and ϵ is a parameter indicating the reconnection speed, $v_c = \epsilon v_A$, where $v_A \approx c$ is the Alfvén velocity [9]. Note that, for $\sigma \approx 10^4$, $R_{\mathrm{mag}} \approx 10^{16}$ cm, typical of LGRB prompt emission radii. Metzger et al. 2010 [9] estimate this transition to a large magnetization will happen at slightly less than 60 seconds after magnetar birth for a magnetar with a mass of $M_\odot$, a dipole magnetic field of 10^{15} G and an initial period of roughly 1 ms.

Metzger et al. 2010 [9] consider two possibilities for prompt emission mechanisms: magnetic dissipation resulting in baryon in accelerating with reconnection responsible for emission, and magnetic dissipation accelerating baryons with subsequent internal shocks resulting in the prompt emission. This are discussed further in Sec. 3.2). In either case, magnetic dissipation is likely responsible for the acceleration mechanism.

Prompt emission also determines the period at the beginning of the afterglow phase. This gives us the initial period conditions in the afterglow phase, where dipole radiation is assumed to dominate the lightcurve evolution.

In Fig. 1, we plot the period evolution during the prompt emission phase following different expressions for energy loss assuming no mass fallback. We assume a magnetar with radius 12 km, initial period at onset of prompt emission of 1 ms, and a mass of 2 $M_\odot$. We consider both the upper and lower limits of $\dot{E}$ in Fig. 2 in Metzger et al. 2010 [9], where $\dot{E}$ is the wind power at large radii (see Eq. 23), consisting of both magnetic and kinetic energy. For comparison, we also plot what the period would be if dipole radiation were the only source of spidown. The period evolution is significant only in the case of strong wind radiation corresponding to an energy loss rate $\dot{E} = 7 \times 10^{50}$ erg s^{-1}, in which case we expect the magnetar to spin down to ~ 3 s by the end of prompt emission.

In Fig. 2, we plot the period evolution during the prompt emission phase for a magnetar with the same initial parameters as above, but we now allow for mass fallback such that the magnetar is in the propeller regime, $r_m > r_c$, during this phase. In contrast to Fig. 1, the period evolution is dominated both by a dipole spindown and by possibly a strong wind corresponding to $\dot{E} = 7 \times 10^{50}$ erg s^{-1}. If we naively assume that these two processes are decoupled, we expect the magnetar to spin down to roughly 5 ms at the end of prompt emission. However, even in the case of negligible wind radiation, the magnetar still spins down to ~ 3 ms because it loses angular momentum propelling the fallback mass outwards.

$$\dot{E} = \dot{E}_{\mathrm{kin}} + \dot{E}_{\mathrm{mag}} \approx \begin{cases} \dot{M}c^2\sigma^{2/3} & \text{if } \sigma \ll 1 \\ (2/3)\dot{M}c^2\sigma & \text{if } \sigma \gg 1 \, . \end{cases} \tag{23}$$

3.2 Thermalization: Dissipation vs Shocks

Magnetic energy can be dissipated by reconnection (see Sironi & Spitkovksy et al. 2014 [35] and Melzani et al. 2014 [36]), which can either heat plasma and accelerate baryons locally (see Lyutikov & Blandford 2003 [37]) or drive bulk motions and excite plasma turbulences to heat the plasma on a larger scale (see Thompson 1994 [38]).

In this case, magnetic dissipation results in both acceleration and thermalization of the energy initially available in the Poynting flux. Electron temperatures exceed equilibrium temperature [9], resulting in inverse Compton scattering. Synchotron scattering may also occur at lower frequencies, softening the LGRB spectra [9].

Prompt emission powered by magnetic dissipation is thought to end when reconnection is no longer able to efficiently occur before the typical LGRB prompt emission radii (see Sec. 3.1). As argued in Sec. 3.1, a magnetization $\gtrsim 10^4$ is sufficient to increase $R_{mag} \gtrsim 10^{16}$ cm, the typical prompt emission radius. At this magnetization, insufficient acceleration and dissipation occurs before emission is expected even if reconnection were to occur at light speed, causally constraining prompt emission duration associated with magnetic dissipation [34]. The prompt emission timescale in the case of internal shocks is similarly constrained, as we will show below.
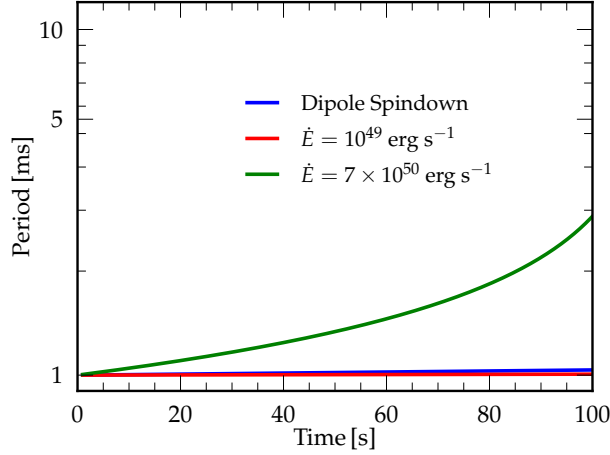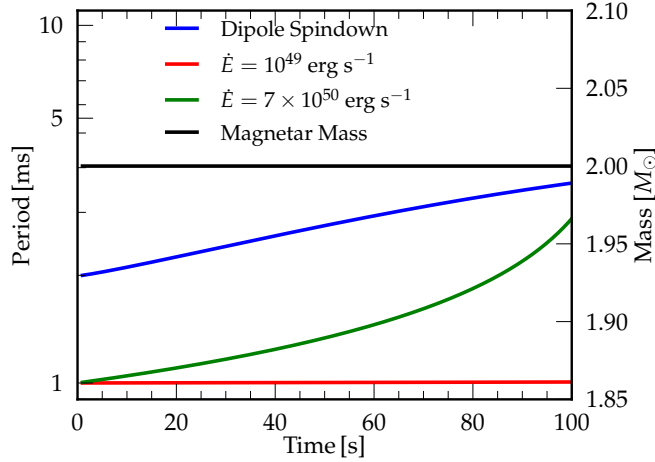
Figure 1: We plot the period evolution in the prompt emission phase for a magnetar with mass of 2 $M_\odot$, radius 12 km and magnetic field of 10^{15} G. The magnetic axis is assumed orthogonal to the dipole axis, and mass fallback is neglected. We compare the period evolution using the limits of Fig. 2 of Metzger et al. 2010 [9] to the dipole spindown case. In the extreme case, assuming the upper limit in Fig. 2 in Metzger et al. of $\dot{E} = 10^{51}$ erg s^{-1}, the period increases to 3 ms. For both the lower limits and dipole radiation alone, the period decay is negligible. This limits are derived assuming the magnetar loses energy at a rate, $\dot{E}$ dominated by a kinetic energy and a Poynting flux. See text for details.

Figure 2: We plot the period evolution in the prompt emission phase for a magnetar with mass of 2 $M_\odot$, radius 12 km and magnetic field of 10^{15} G. The magnetic axis is assumed orthogonal to the dipole axis, but we allow for mass fallback such that the magnetar is in the propeller regime, $r_m > r_c$ and accretes no mass. We compare the period evolution using the limits of Fig. 2 of Metzger et al. 2010 [9] to the dipole spindown case. This limits are derived assuming the energy loss rate, $\dot{E}$, is dominated by a kinetic energy and a Poynting flux. Ther period evolution is now dominated by both a propeller wind and dipole spindown. If we assume that these processes are decoupled, the magnetar will spindown to a period of ~ 5s by the end of prompt emission. See text for details.

Metzger et al. 2010 [9] define internal shocks differently than usually ascribed to the fireball model. Rather than considering internal shocks from ejecta shells released immediately after one another and moving at different velocities, Metzger et al. consider the magnetar jet interacting with a slower shell of

accummulated earlier ejecta. Since the Lorentz factor increases with time for large magnetization, the accummulation model for internal shocks is favored over the adjacent shell collision model.

Below we show that the Lorentz factor scales linearly with the magnetization for $\sigma \gg 1$ and thus increases with time through the prompt emission phase. The maximum Lorentz factor, Γ_{max} requires that the entire energy available, E, be converted into kinetic energy,

$$E = (\Gamma_{\mathrm{max}} - 1)Mc^2 \approx \Gamma_{\mathrm{max}}Mc^2 \ , \tag{24}$$

for $\Gamma_{\mathrm{max}} \gg 1$, and we expect $\Gamma_{\mathrm{max}} \approx 100$ for prompt emission. So, $\Gamma_{\mathrm{max}} \approx E/Mc^2 \approx \dot{E}/\dot{M}c^2$. However, $E = \dot{E}_{\mathrm{kin}} + \dot{E}_{\mathrm{mag}} \approx \frac{2}{3}\dot{M}c^2\sigma$ for $\sigma \gg 1$ following Metzger et al. 2010 [9]. Comparing, we see that for large magnetization, $\sigma \approx \Gamma_{\mathrm{max}}$ and since magnetization increases through prompt emission, so will the Lorentz factor.

We then consider the radius where internal shocks occur. Eq. B3 in Metzger et al. 2010 [9],

$$R_{\mathrm{is}} \approx 2\Gamma_s^2 ct_j \left(1 - \frac{1}{2\Gamma_s^2}\right) \ , \tag{25}$$

which is accurate for an ultrarelativistic jet with Lorentz factor Γ_j colliding with slower but also ultrarelativistic accumulated mass ejected earlier, with Lorentz factor Γ_s. Eq. 25 holds for $\Gamma_j \gg \Gamma_s$. In the internal shock emission model, prompt emission ends when $R_{\mathrm{mag}} \gg R_{\mathrm{is}}$ since the ejecta will no longer be sufficiently accelerated before the internal shock radius. Thus, a high magnetization (and hence a large R_{mag}) similarly ends prompt emission in this scenario.

However, Metzger et al. 2010 [9] prefer magnetic dissipation to internal shocks as the model for prompt emission for two reasons. First, the peak spectral energy increases as a function of time for the internal shock model, whereas peak energy remains roughly constaint in actual bursts. Second, from Eq. 25, we can estimate the variability timescale of the prompt emission lightcurve for the internal shock model as $\delta t \propto t \propto R_{is}/2\Gamma_s^2$. This timescale increases linearly with time, whereas observations indicate that the variability timescale varies weakly during the burst [39].

4   Afterglow and Plateau

In Sec. 4.1, we summarize the argument in Lyons et al. 2009 illustrating the dipole model in powering a lengthy plateau in the afterglow of an LGRB lightcurve. In Sec. 4.2, we explore possible scenarios involving a magnetar as an LGRB central engine. In Sec. 4.3, we study the roles of magnetar spindown and mass fallback in determining magnetar stability against gravitational collapse.

4.1   Lyons et al. 2009: Spindown Powered Plateau

We explore the argument in Lyons et al. 2009 [29] that plateau features lasting $100\,\mathrm{s}$ to $1000\,\mathrm{s}$ of seconds in LGRB afterglows can be explained by the dipole radiation model of a magnetar. As a first order estimate, we trace the steps in Lyons et al. and neglect fallback accretion. Following Piro & Ott 2011 [26] and neglecting spindown from fallback accretion, we have

$$I\dot{\Omega} = N_{\mathrm{dip}} \ , \tag{26}$$

where $N_{\mathrm{dip}} = -\mu^2\Omega^3/6c^3$, assuming $\alpha = \pi/2$. We solve for angular velocity as a function of time,

$$\Omega(t) = \frac{\sqrt{\frac{21}{2}}c^{3/2}\sqrt{M}R}{\sqrt{10t\mu^2 - 21c^3MR^2y}} \ . \tag{27}$$

Together with Eq. 8, we can solve for spindown radiation luminosity as a function of time, arriving at

$$L_{\mathrm{dip}} = \frac{147B^2c^3M^2R^{10}}{8(-21c^3MR^2y + \frac{5}{2}B^2R^6t)^2} \ , \tag{28}$$

where we have used $\mu = BR^3/2$, the magnetic moment for a uniformly magnetized sphere, and y is a negative value related to initial period P_o by $P_o = 2\pi\sqrt{-2y}$.

Note the interesting result that luminosity may actually decrease with increasing magnetic field at a given time. A stronger field brakes the magnetar, decreasing its spin frequency as seen in Eq. 27. Since frequency comes in with the inverse 4th power, while the magnetic field comes in only with the 2nd power in Eq. 8, luminosity may indeed decrease with higher magnetic field.

We correct for anistropic emission using Eq. 5 of Lyons et al. 2009 [29],

$$E_{\text{beam}} = (1 - \cos\theta_b)E_{\text{iso}} , \tag{29}$$

where θ_b is the jet's half opening-angle and indicates how narrowly it is beamed. Conventionally, it is measured as the angle between the magnetar spin axis and the outer axis of the jet, which is preferentially driven along the rotation axis [22]. We assumed that this does not change with time, thus the analogous correlation holds for luminosity. In defining the jet beam angle, we assume that the spin and dipole axes are aligned, yet this would produce no radiation unless we follow Spitkovsky's model discussed earlier.

The beaming angle is derived by performing a spherical integral to derive the beaming fraction, f_b, of the neutron star,

$$f_b = \frac{\int_0^{2\pi} \int_0^{\theta_b} \sin(\theta)d\theta d\phi}{\int_0^{2\pi} \int_0^{\pi/2} \sin(\theta)d\theta d\phi} = 1 - \cos\theta_b . \tag{30}$$

4.1.1 Assumptions

Lyons et al. 2009 [29] assume $1.4M_\odot$ for the magnetar mass. She identifies an LGRB lightcurve with a lengthy plateau phase that immediate cuts off as noncanonical. Such noncanonical LGRBs constitute 10% of all observed LGRBs [29]. The noncanonical model demands magnetar collapse to a black hole to shut off the light curve, but a $1.4M_\odot$ neutron star will not collapse to a BH. Furthermore, it is uncertain how a magnetar will reach initial spin periods of 1 ms.

4.1.2 K-correction

Since GRBs occur at significant redshifts, the source restframe X-ray afterglows are shifted appreciably towards lower frequencies. We K-correct (from the German *Konstante*, coined in 1918 by astronomer Carl Wilhelm Wirtz) the detected bandpass into the rest frame of emission. The spectral indices Γ are available from SWIFT at [40]. The spectral index β defines the spectral evolution of the flux, $f(\nu) \propto \nu^{-\beta}$ and is simply $\Gamma - 1$. From Hogg 2002 [41], the K-corrected luminosity is then:

$$L_{[.3-10keV]} = 4\pi f_{[.3-10keV]}d_L^2(1+z)^{-1+\beta} , \tag{31}$$

where we use 0.3-10 keV as the X-ray bandpass. $L_{[.3-10\,keV]}$ is the luminosity in this bandpass calculated from the Swift flux data, $f_{[.3-10\,keV]}$. z is the LGRB redshift and d_L the luminosity distance of the LGRB. Redshifts are available at [42] and were verified with original references. The luminosity distancew was calculated using Ned Wright's JavaScript cosmology calculator available at [43] for the Standard Cosmological Model.

4.2 Possible Scenarios Involving a Magnetar as GRB Central Engine

In the following, we identify and briefly summarize different models that can explain plateau features in the afterglows of magnetar lightcurves. They will be discussed in greater detail in Sec. 4.3.

- We can have a plateau and apparent cutoff explained entirely by the dipolespindown model. For instance, see Fig. 9. Gravitational collapse is not required to explain plateau decay and accretion is not considered. Rather, the dipole spindown model's curvature can explain the plateau feature. Recall from Eq. 9 that the luminosity for the dipole spindown model scales as P^{-4}, where P is the period at the beginning of the afterglow. Thus the decay of a plateau may in some cases be

explained entirely by the decaying period of the magnetar. In Fig. 9, we show examples of the dipole spindown model accounting for both the duration of a plateau lasting from several hundred to over a thousand seconds and the steep cutoff shortly afterwards. Note from Eq. 10 that the dipole spindown time roughly scales as B^{-2} where B is the magnetar magnetic field in the dipole spindown model. In Fig. 9a−Fig 9c, we see that magnetars with magnetic fields $> 10^{15}$ G cannot power a plateau of $1000\,$s.

- We can have accretion induced collapse to a blackhole for a variety of magnetar initial masses, magnetic fields, initial spin periods, and accretion parameters $0.1 - 10$. Our maximum mass for a given period is constrained by the HShen EOS in Fig. 5. Together with Fig. 7, we can constrain w. Or, we may have the inverse situation, spindown collapse without mass accretion. In such a case, an initially rotationally supported supramassive magnetar slows until centrifugal support is no longer able to sustain the magnetar even in the absence of accretion.

  We may initially have a hypermassive, $\gtrsim 2.5\ M_\odot$, differentially rotating magnetar. However, bar mode, magnetic, and other instabilities will redistribute angular momentum to make the magnetar rigidly rotating within the first second. Thus the above collapse arguments still apply (citation needed).

- We may also have no collapse and see a plateau lasting upwards of $1000\,$s, or immediate collapse and thus no plateau or a much fainter one. Such examples will provide the basis for a statistical distribution of magnetar powered LGRBs. In Fig. 3, we plot the fluences of two such observed LGRBs. In Fig. 3a, we illustrate an LGRB with no observable plateau. Such an LGRB is possible if, for instance, the magnetic field is $> 10^{15}\,$G. From Eq. 10, we know that the characteristic timescale for spindown $\propto B^{-2}$ absent mass fallback. Thus, we may be seeing the tail-end of the dipole spindown model for a magnetar with a larger magnetic field. In Fig. 3b, we plot an LGRB whose flux declines by ~ 5 orders of magnitude in the first $300\,$s then remains roughly constant for $\sim 3 \times 10^5\,$s. One such possibility, which we do not explore in this paper, is if a magnetar powering an LGRB collapses on a timescale of $\sim 100\,$s to a black hole, accretion onto which then powers a lightcurve plateau many orders smaller than the prompt emission. Possible causes may be the loss of angular momentum in the resulting BH or simply a steep decay in available mass for accretion. Both are reasonable estimates. As we show in Fig. 7, magnetars are expected to spindown sufficiently within the first $\sim 100\,$s, and the bulk of acccretion often happens in the first hundred seconds of the magnetar's activity, as seen in Fig. 7 & 10.

  The GRB data is available at Swift [40].

In the subsequent section, we explore the first two possibilities in greater detail.

4.3 Centrifugal Support and Black Hole Formation

We explore the possibility of magnetar spindown and mass fallback until rotational support is insufficient to prevent gravitational collapse.

As an order of magnitude estimate we plot in Fig. 4 the ratio of the centrifugal force over the gravitational force at the outer radius of the magnetar as a function of magnetar period. Though the radius may evolve during the first few seconds (see Metzger et al. 2010 [9]), it is reasonable to assume that the radius remains constant during the afterglow phase.

Note how, by a period of a few milliseconds, the centrifugal support has declined by several orders of magnitude. We are curious whether the magnetar has spindown sufficiently and/or accreted sufficient mass to collapse into a black hole. In Fig. 5, we plot the maximum baryon mass for a given magnetar period for the HShen equation of state (see HShen et. al 2012 [44]). For context, in Fig. 6, we plot the period evolution of magnetars neglecting mass fallback and assuming only dipole spindown. We see that, for magnetic fields $\lesssim 10^{15}$, an initial period of $1\,$ms decays negligibly (remains $\ll 2\,$ms). However, recall
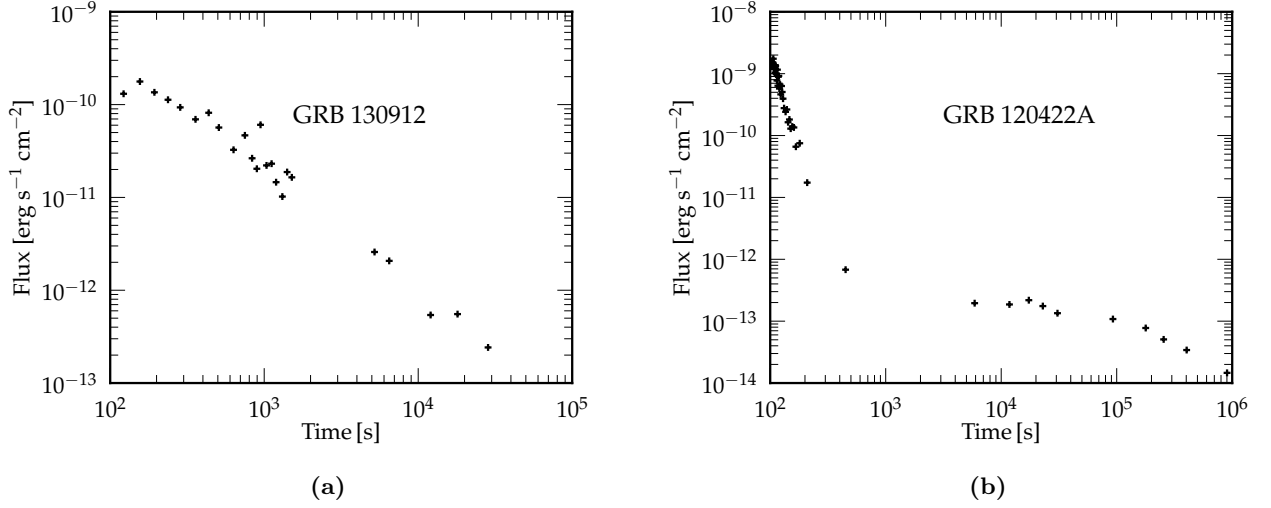
Figure 3: Fluences for two LGRBs. The left panel, GRB 130912, is an example of an LGRB with no observable plateau. The flux decays almost monotonically for the entire observed duration. The right panel, GRB 120422A decays rapidly in the first $100\,\mathrm{s}$, then remains roughly constant for the next several $10^5\,\mathrm{s}$. We briefly discuss central engine possibilities in the text.
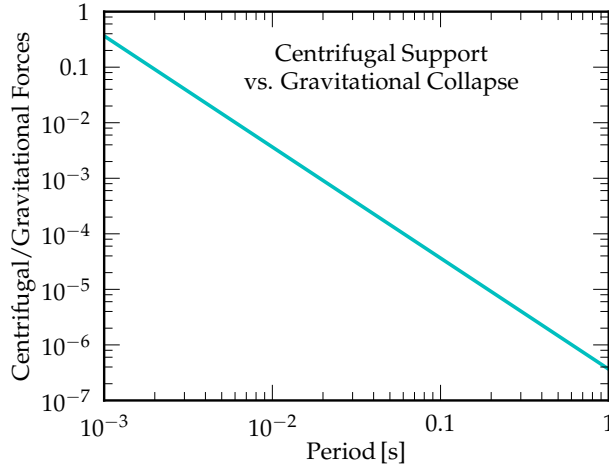

Figure 4: Newtonian estimate of the centrifugal support against gravitational collapse as a function of period on the equatorial surface of the NS, which we assume to be spherically symmetric. We use a $1.4\ M_\odot$ NS with a 12 km radius and neglect fallback accretion.

from Eq. 9 that the dipole luminosity scales as B^2. Consequently, a magnetic field much smaller than $10^{15}\,\mathrm{G}$ may not be able to power observed LGRB lightcurves. We explore the magnetar luminosities for a dipole spindown model in Fig. 9.

Next we consider fallback accretion. In Fig. 7 below, we use the notation rXmYbZ where X is the radius in km, Y is the mass in solar masses and Z indicates the dipole magnetic field in 10^Z Gauss. η is our accretion parameter described above associated with the supernova's efficiency in stripping the stellar envelope. A smaller η signifies less fallback.

In Fig. 7a, we see that if the magnetar does not collapse within the first 10 seconds, it may power an afterglow lasting up to a 1000 seconds since the period remains roughly constant until then, doubling to $2\,\mathrm{ms}$ at $\sim 1000\,\mathrm{s}$. In Fig. 7b, we increase the initial mass. The magnetar spins down significantly
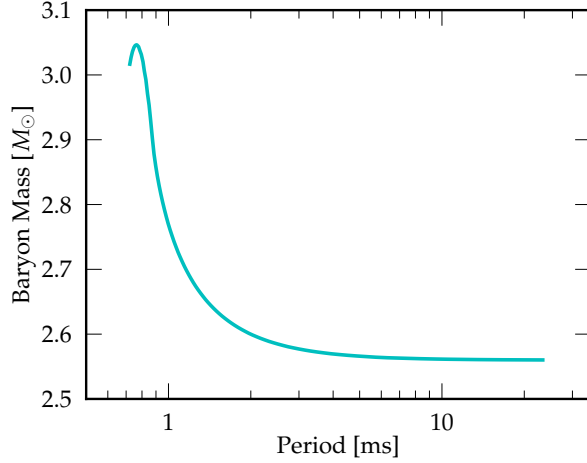
Figure 5: Maximum baryonic mass as a function of period for HShen EOS [44]. Doubling the period from 1 ms to 2 ms reduces maximum supported mass from just over 3.0 $M_\odot$ to 2.6 $M_\odot$. Maximum supported mass plateaus at just under 2.6 $M_\odot$. From Fig. 1 we expect a magnetar in the propeller regime to spindown to $\sim 5\,\mathrm{s}$, with a corresponding maximum mass of $\sim 2.57 M_\odot$.
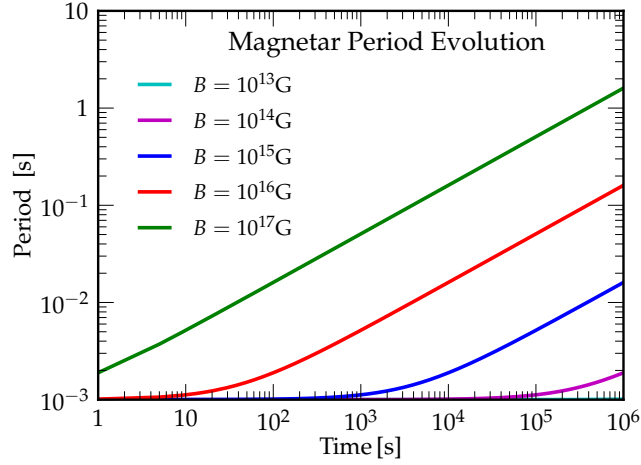

Figure 6: Magnetar period evolution due to magnetic dipole spindown for a spherically symmetric neutron star with an initial period of 1 ms at the beginning of prompt emission, radius of 12 km, and a mass of $1.4 M_\odot$. We neglect fallback accretion and assume the rotation axis is orthogonal to the dipole axis.

between 100 and 1000 seconds, but accretes no mass. However, from Fig. 5, we know that a magnetar with period $\gtrsim$ than 2 ms cannot support more than $2.6 M_\odot$ of baryonic mass, and thus we expect this magnetar to collapse at $\sim 200\,\mathrm{s}$. In Fig. 7c, we reduce the magnetic field to $10^{14}\,\mathrm{G}$. Recall from Eq. 10 that the spindown time scales as B^{-2} in the dipole limit, and we expect a magnetar to be dominated by the dipole model at late times. As expected, we see dipole decay dominate at $\sim 10^4\,\mathrm{s}$. From Fig. 5, we know that a magnetar with a period of 1 ms can survive up to a mass of $\sim 3.1 M_\odot$, and thus we expect our magnetar to survive up to 1000 s against gravitational collapse. However, the magnetar may become rotationally unstable around several hundred seconds due to fallback accretion spinning the magnetar up. In Fig. 8, we check for rotational stability in the non-Newtonian limit following Lattimer & Prakash
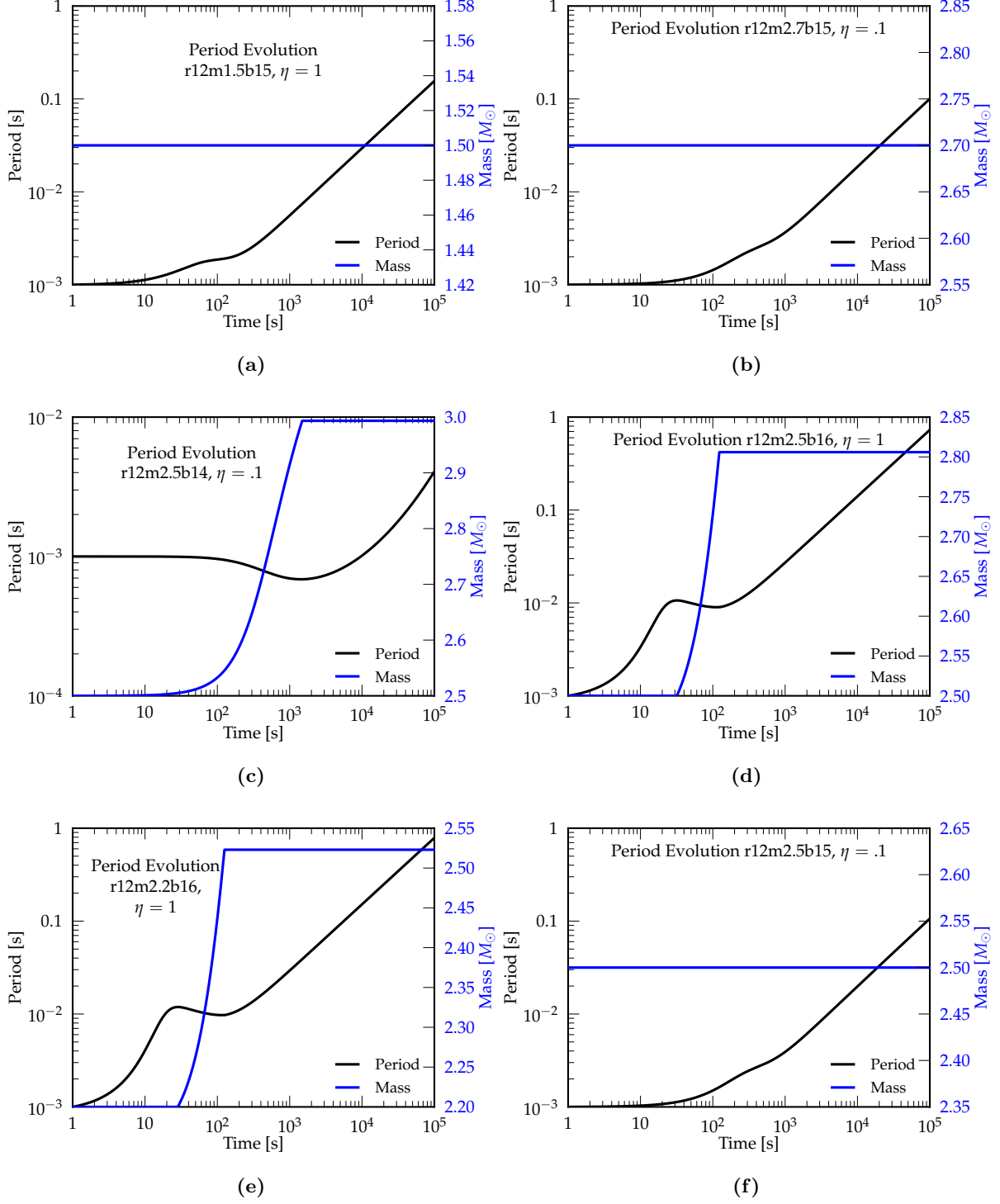
Figure 7: Magnetar periods evolved under dipole spindown assuming mass fallback. The magnetar has an initial period of 1 ms at the beginning of the afterglow phase and we explore a range of initial masses and magnetic fields. We also vary η, which parametrizes the mass fallback rate. See text for details.

2001 [30]. We use $T = I\Omega^2/2$ and

$$|W| \approx 0.6Mc^2 \frac{GM/Rc^2}{1 - 0.5(GM/Rc^2}$$
(32)

16

to calculate the rotation parameter $\beta = \mathrm{T}/|W|$. For reference, at $\beta = 0.5$, the neutron star is at breakup and can no longer gain angular momentum. Dynamical bar-mode instabilities occur at $\beta > 0.27$ and secular instabilities at $\beta > 0.14$. The instabilities are accepted to radiate or re-adjust angular momentum and thus set $N_{acc} = 0$ (see Eq. 17 and Eq. 18). Even though the magnetar model in Fig. 7c spins up to ~ 0.7 ms, from Fig. 8 we see that the magnetar will still be rotationally stable since its rotation parameter peaks under 0.1, short of even secular instabilities regime.

In Fig. 7d, we instead increase the magnetic field to 10^{15} G. Consequently, dipole spindown dominates earlier, at ~ 200 s. The magnetar both spins down significantly and accretes significantly. From Fig. 5, we do not expect this magnetar to survive against collapse to 1000 s, when it will have a period of ~ 10 s and a mass of $\sim 2.8 M_\odot$. For comparison, in Fig. 7e, we plot the period evolution of a magnetar with the same parameters as that in Fig. 7d but with a smaller initial mass of 2.2 $M_\odot$. This magnetar is expected to survive indefinitely against gravitational collapse. Similarly, in Fig. 7f, we plot the period evolution of a magnetar with the same parameters as that in Fig. 7b, but with a smaller initial mass of 2.5 $M_\odot$. This examples illustrate that the magnetar's survival against gravitational collapse is highly sensitive to its initial mass and mass accretion, and its spindown at late times is highly sensitive to the magnetic field.
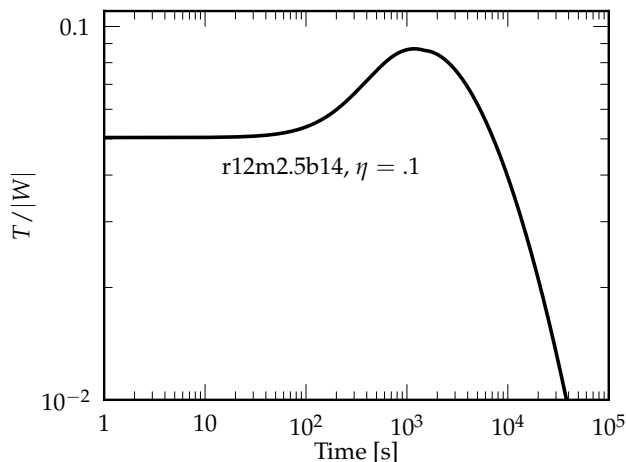

Figure 8: We plot $\beta = \mathrm{T}/|W|$ to check the rotational stability for the magnetar in Fig. 7c with initial period of 1 ms at the beginning of the afterglow phase, an initial mass of 2.5 $M_\odot$, and a magnetic field of 10^{14} G. We calculate $\mathrm{T}/|W|$ in the non-Newtonian limit following Lattimer & Prakash 2001 [30]. β peaks under 0.1, short of the rotation parameter where any instabilities occur, and thus we expect the magnetar to be rotationally stable. See text for details.

In Fig. 9, we compare LGRB lightcurves with the dipole model. We neglect fallback accretion and assume a radius of 12 km. The figure illustrateslight curves using data from Swift in the $0.3 - 10$ keV bandpass. Following Lyons et al. 2009 [29], we use beaming angles between $1°$ and a few tens of degrees [29]. In Fig. 9a-9c, we compare afteglow lightcurves for a variety of dipole spindown models, varying magnetic field, mass, and beaming angle. We assume period of 1 ms at onset of the afterglow phase. Figures 9d-9e are fit explicitly to the dipole spindown model for magnetic field, mass, beaming angle, and period at onset of the afterglow phase, rather than constrained by an array of parameters. See Fig. 9 caption for further details. The key point is that, for typical values of magnetar magnetic fields, initial periods, and beaming angles we can reproduce energies of observed LGRBs without fine-tuning parameters.

In Fig. 10, we add mass fallback to our magnetar period evolution. In Fig. 10a, we assume fallback accretion with sufficient material and the absence of a propeller regime. As seen in Fig. 10a, depending on the supernova explosion strength, magnetars may accrete several solar masses $M_\odot$ in the first several hundred seconds. In Fig. 10b, we plot mass accretion and the fastness parameter for a magnetar with a particularly high 5 ms initial period, initial mass of 2 $M_\odot$ and a field of 10^{15} G. The fastness parameter

plotted is $(r_m/r_c)^{3/2}$ and determines whether the magnetar is in the propeller regime (where the fastness parameter is greater than 1). Interestingly, if we decrease the period to 1 ms, the magnetar is always (at least until 10^7 seconds) in the propeller regime and does not accrete.

Additionally, we plot in Fig. 11 the ratio of centrifugal to gravitational forces as a function of time and period to determine stability against gravitational collapse. The magnetar spins up at several hundred seconds due to fallback accretion transferring angular momentum to the magnetar. Though Fig. 11 indicates that the magnetar has not spun down appreciably even at 1000 seconds, it has by then accreted over 0.5 $M_\odot$ of material. However, from Fig. 5, we see that the magnetar is still rotational supported and under its maximum baryon mass before collapse. Together with Fig. 2, Fig. 11 fully illustrates the complete period evolution of an LGRB from onset of prompt emission through an afterglow plateau lasting over 1000 s. Such a magnetar is initially in the propeller regime during the prompt emission, slowing down to a period of 1 ms by 100 s, when we assume prompt emission ends and afterglow begins according to the discussing of magnetization's role on prompt emission longevity earlier. During the afterglow phase, the magnetar transitions to an accreting regime, spinning up to a period of ~ 2 ms by several hundred seconds before dipole spindown dominates the period evolution. Such a magnetar can be expected to reproduce typical LGRB durations. Then, together with the luminosities plotted in Fig. 9, we expect that such a magnetar will also be able to further reproduce typical LGRB energies. No parameter fine-tuning was required to identify such a magnetar, and we further stipulate that a wide variety of garden-variety magnetars will be able to reproduce a more complete spectra of observed LGRBs.

5   Conclusion

Existing literature (see Woosley et. al 2006 [10] and Bernardini et al. 2013 [17]) show the magnetar formation among the SNe 1bc population correlates with the LGRB rate in the same population, and that the magnetar's rotational energy is sufficient to power an LGRB.

We have further identified magnetar masses, initial prompt emission periods, and magnetic fields that allows for prompt emission phases lasting up to 100 s and afterglow phases lasting up to 1000 s. In particular, we have illustrated that a magnetar in the propeller regime for the first 100 s may result in a smaller magnetization in its local environment and hence increase the longevity of prompt emission. This propeller regime also prevents early accretion-induced collapse into a black hole. The magnetar may then transition into an accretion regime or remain in the propeller limit. In the latter case, subsequent accretion will spin up the magnetar, possibly sustaining the magnetar against gravitational collapse until it accretes to a mass of $3M_\odot$. In either case, the magnetar will survive until it is no longer centrifugally supported, owing either to mass accretion, magnetar spindown, or both. We subsequently calculated the allowed maximum masses for a given EOS and angular velocity following Kaplan et al. 2013 [45]. We then identified examples of magnetars centrifugally supported against gravitational collapse for ~ 1000 s and thus capable of powering lightcurve plateaus of equal duration.

Others have done similar work in identifying the magnetar as a central engine for LGRBs. Metzger et al. 2010 [9] follow a similar model of an early Poynting flux outflow and a dipole wind powering the prompt emission, neglecting mass accretion. Lyons et al. 2009 [29] account for a lengthy plateau by citing magnetic dipole emission as well. In contrast, Bernardini et al. 2013 [17] cite magnetar accretion as powering the prompt emission, and a dipole wind the afterglow. Bucciantini et al. 2007 [22] model the initial magnetar in a cavity and simulate a relativistic jet forming in the intial vacuum. Yet, our approach is unique in assuming a magnetar situated in a non-cavity, with early energy outflow dominated by a Poynting flux that subsequently thermalizes to produce prompt emission. Furthermore, we assume a mass accretion model that may increase prompt emission longevity and also affects dipole spindown in the afterglow phase. Finally, our approach both models magnetars capable of suriving upwards of 1000 s as well as fitting observed LGRBs to our models.

Our work was limited to a vanilla analysis of magnetar models in predicting LGRB energies and durations. Further work identifying spectral characteristics of lightcurves, exploring spectral features of LGRB associated SN, and fundamental nuclear physics comparing emission models for magnetar-powered LGRB vs BH-powered LGRBs can be done to either support or disprove the magnetar model

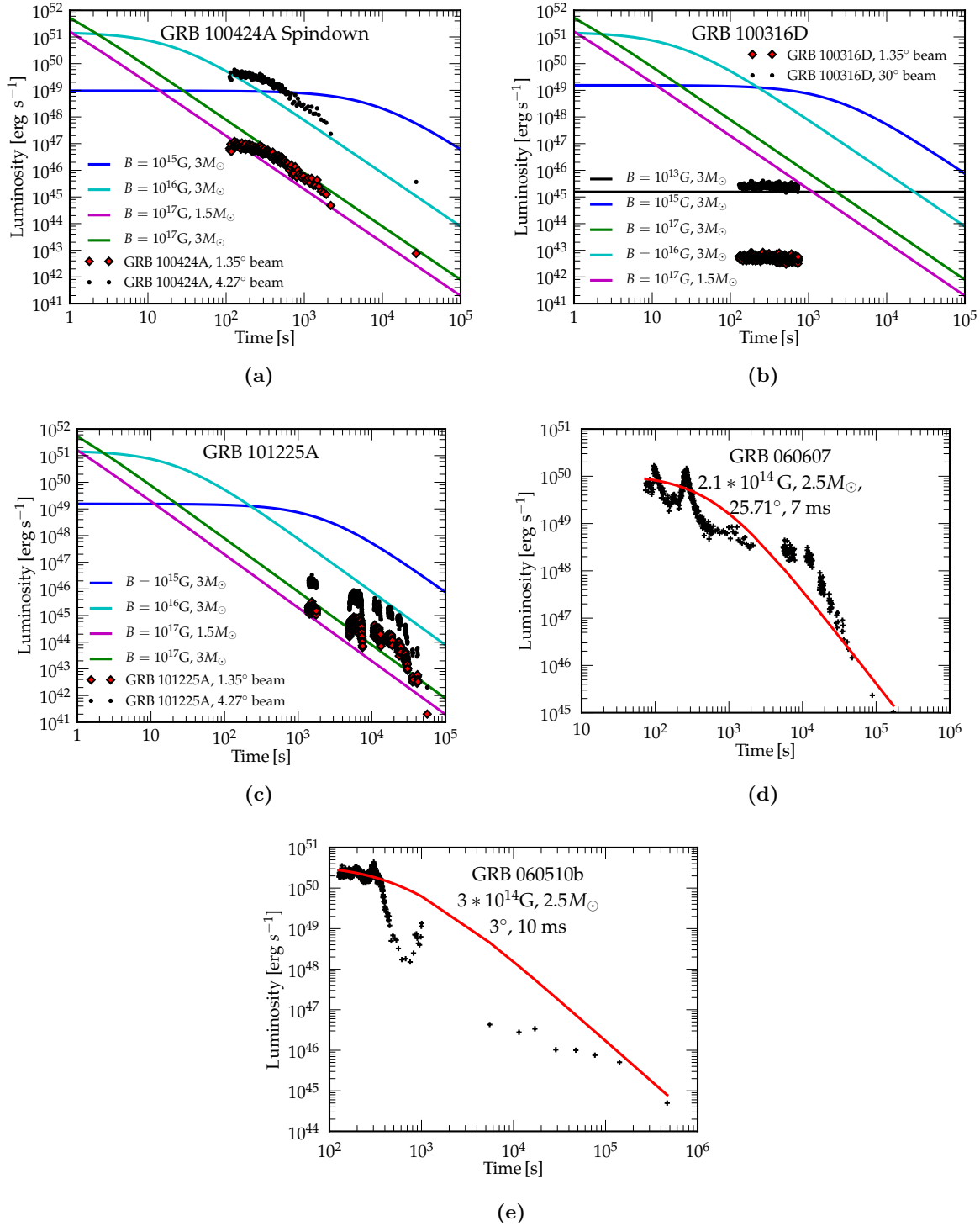for LGRB central engines.

6   Acknowledgements

Figure 9: We plot actual LGRB lightcurves against the dipole spindown model for the given parameters, neglecting mass fallback. In the first three panels, we plot afterglows of actual LGRB lightcurves from SWIFT against various models for magnetar mass, beaming angle, and magnetic field. We assume a period of 1 ms at the beginning of the afterglow. Due to the limited observational afterglow data of GRB 100316D shown in the top right panel, we cannot extrapolate an accurate beaming angle. In the last two panels, we perform a least squares fit of SWIFT LGRBs, varying magnetic field, period, mass, and beaming angle. These two plots began at a a later time corresponding to the beginning of the afterglow phase of the LGRBs. The two early peaks in the middle right panel are likely flares, increased activity of the central engine for a short period of time. The luminosity decay of nearly two orders of magnitude in the bottom panel may be evidence of early collapse to a black hole at several hundred seconds following by a flare, perhaps powered by accretion onto the black hole.
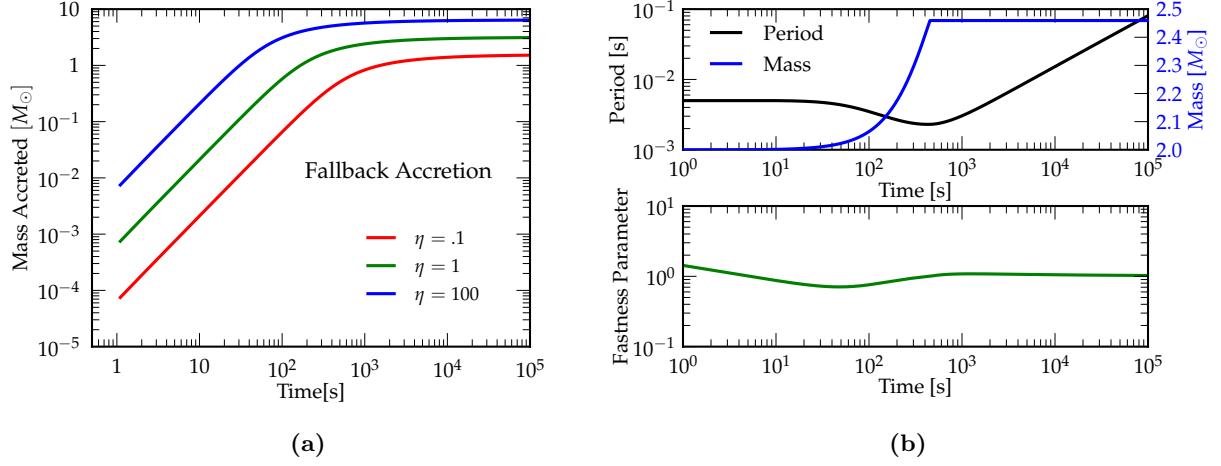
Figure 10: In the left panel, we plot mass accretion in the absence of a propeller regime, so $r_c > r_m$ for all relevant times. In the right panel, we plot the period and fastness parameter for a spherically symmetric magnetar with initial mass of 2 $M_\odot$, magnetic field of 10^{15} G, radius of 12 km, $\eta = 0.1$, and period 1 ms at the beginning of prompt emission. Though the magnetar period does not decay appreciably for the first 1000 s, the magnetar accretes over half a solar mass during that time, so its survival depends sensitively on the neutron star equation of state.
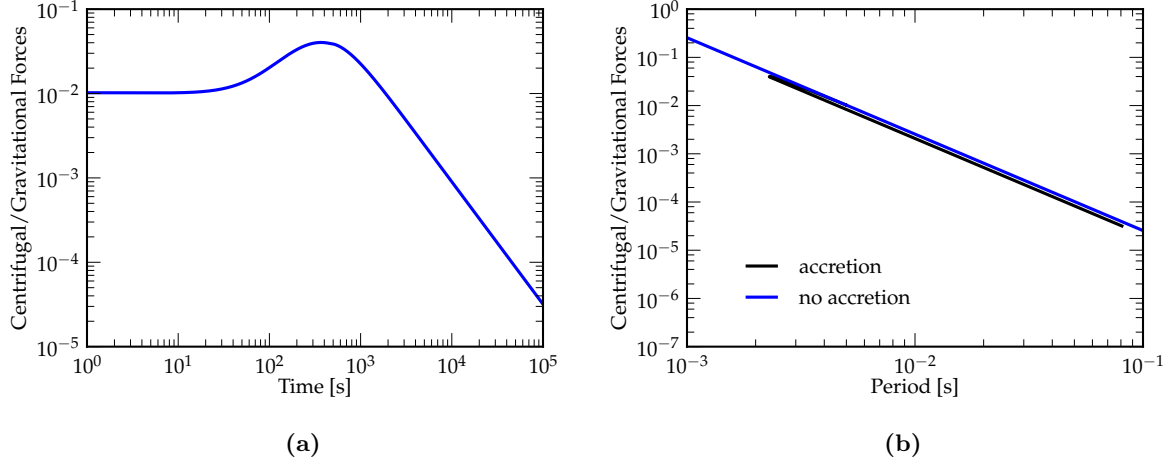

Figure 11: We plot centrifugal support for the magnetar with initial mass of 2 $M_\odot$, magnetic field of 10^{15} G, radius of 12 km, $\eta = 0.1$ and a period of 5 ms at the beginning of the afterglow phase. In the left panel, we plot centrifugal support against gravitational collapse as a function of time. The magnetar is spun up at several hundred seconds. We see a bump at several hundred seconds as fallback accretion spins up the magnetar. In the right panel, we plot centrifugal support against gravitational collapse as a function of period. Note that the centrifugal support is a factor of several smaller in the accreting case than in the non-accreting case.

21

7   References

[1] Dr. Barbara Mattson. Gamma Ray Bursts. `http://imagine.gsfc.nasa.gov/docs/science/know_l1/bursts.html`, 2013. [Online].

[2] C. Kouveliotou, C.A. Meegan, G.J. Fishman, N.P. Bhat, M.S. Briggs, T.M. Koshut, W.S. Paciesas, and G.N. Pendleton. Identification of two classes of gamma-ray bursts. *Astrophys. J*, 413:L101–L104, 1993.

[3] Ying Qin, En-Wei Liang, Yun-Feng Liang, Shuang-Xi Yi, Lin Lin, Bin-Bin Zhang, Jin Zhang, Hou-Jun L, Rui-Jing Lu, Lian-Zhong L, and Bing Zhang. A Comprehensive Analysis of Fermi Gamma-Ray Burst Data. III. Energy-dependent T 90 Distributions of GBM GRBs and Instrumental Selection Effect on Duration Classification. *Astrophys. J*, 763:15, 2013.

[4] A.J. Levan, P. Jakobsson, C. Hurkett, N.R. Tanvir, J. Gorosabel, et al. A case of mistaken identity? GRB 060912A and the nature of the long – short GRB divide. *Mon.Not.Roy.Astron.Soc.*, 378:1439–1446, 2007.

[5] Takashi Nakamura, Kazumi Kashiyama, Daisuke Nakauchi, Yudai Suwa, Takanori Sakamoto, et al. Soft X-ray Extended Emissions of Short Gamma-Ray Bursts as Electromagnetic Counterparts of Compact Binary Mergers; Possible Origin and Detectability. 2013.

[6] Ben Gompertz, Paul O'Brien, Graham Wynn, and Antonia Rowlinson. Can magnetar spin-down power extended emission in some short GRBs? 2013.

[7] A. Rowlinson, P.T. O'Brien, Tanvir N.R., B. Zhang, P.A. Evans, N. Lyons, A.J. Levan, R. Willingale, K.L. Page, O. Onal, D.N. Burrows, A.P. Beardmore, T.N. Ukwatta, E. Berger, J. Hjorth, A.S. Fruchter, R.L. Tunnicliffe, D.B. Fox, and A. Cucchiara. The unusual X-ray emission of the short Swift GRB 090515: evidence for the formation of a magnetar? *MNRAS*, 409:531–540, December 2010.

[8] Stephan Rosswog and Marcus Bruggen. *Introduction to High-Energy Astrophysics*. Cambridge University Press, Cambridge, UK, 2007.

[9] B.D. Metzger, D. Giannios, T.A. Thompson, N. Bucciantini, and E. Quataert. The Proto-Magnetar Model for Gamma-Ray Bursts. *MNRAS*, 413:2031–2056, 2010.

[10] S.E. Woosley and J.S. Bloom. The Supernova Gamma-Ray Burst Connection. *Ann.Rev.Astron.Astrophys.*, 44:507–556, 2006.

[11] Peter Meszaros. Gamma-Ray Bursts. *Rept.Prog.Phys.*, 69:2259–2322, 2006.

[12] B. Paczynski. Gamma-ray bursters at cosmological distances. *Astrophys. J*, 308:L43–L46, 1986.

[13] S.G. Djorgovski, S. R. Kulkarni, J.S. Bloom, D.A. Frail, F.A. Harrison, T.J. Galama, D. Reichart, S.M. Castro, D. Fox, R. Sari, E. Berger, P. Price, S. Yost, R. Goodrich, and F. Chaffee. The GRB Host Galaxies and Redshifts. In E. Costa, F. Frontera, and J. Hjorth, editors, *Gamma-ray Bursts in the Afterglow Era*, page 218, 2001.

[14] M. Modjaz. Stellar forensics with the supernova-GRB connection. *Astronomische Nachrichten*, 332:434–447, June 2011.

[15] E. Pian, L. Amati, L.A. Antonelli, R.C. Butler, E. Costa, et al. BeppoSAX observations of GRB980425: Detection of the prompt event and monitoring of the error box. *Astrophys.J.*, 1999.

[16] J. Hjorth and J.S. Bloom. *The Gamma-Ray Burst - Supernova Connection*, pages 169–190. 2012.

[17] Maria Grazia Bernardini, Sergio Campana, Gabriele Ghisellini, Paolo D'Avanzo, Davide Burlon, et al. How to switch on and off a Gamma-ray burst through a magnetar. *Astrophys. J*, 2013.

[18] Bryan M. Gaensler, N.M. McClure-Griffiths, M.S. Oey, M. Haverkorn, J.M. Dickey, et al. A Stellar wind bubble coincident with the anomalous x-ray pulsar 1E 1048.1-5937: Are magnetars formed from massive progenitors? *Astrophys.J.*, 620:L95–L98, 2005.

[19] Dafne Guetta and Massimo Della Valle. On the Rates of Gamma Ray Bursts and Type Ib/c Supernovae. *Astrophys.J.*, 657:L73–L76, 2007.

[20] A.M. Soderberg, S. Chakraborti, G. Pignata, R.A. Chevalier, P. Chandra, A. Ray, M.H. Wieringa, A. Copete, V. Chaplin, V. Connaughton, S.D. Barthelmy, M.F. Bietenholz, N. Chugai, M.D. Stritzinger, M. Hamuy, C. Fransson, O. Fox, E.M. Levesque, J.E. Grindlay, P. Challis, R.J. Foley, R.P. Kirshner, P.A. Milne, and M.A.P. Torres. A relativistic type Ibc supernova without a detected γ-ray burst. *Nature*, 463:513–515, 2010.

[21] Dmitri A. Uzdensky and Andrew I. MacFadyen. Magnetar-Driven Magnetic Tower as a Model for Gamma-Ray Bursts and Asymmetric Supernovae. *Astrophys.J.*, 2006.

[22] N. Bucciantini, E. Quataert, B.D. Arons, J. anddess Metzger, and Todd A. Thompson. Relativistic Jets and Long-Duration Gamma-ray Bursts from the Birth of Magnetars. *Astrophys. J*, 2007.

[23] S.E. Woosley. Gamma-ray bursts from stellar mass accretion disks around black holes. *Astrophys. J*, 405:273–277, 1993.

[24] L. Dessart, E. O'Connor, and C.D. Ott. The Arduous Journey to Black Hole Formation in Potential Gamma-Ray Burst Progenitors. *Astrophys. J*, 754:76, 2012.

[25] Stan Woosley and Alexander Heger. The Progenitor stars of gamma-ray bursts. *Astrophys.J.*, 637:914–921, 2006.

[26] Anthony L. Piro and Christian D. Ott. Supernova Fallback onto Magnetars and Propeller-Powered Supernovae. *Astrophys.J.*, 736:108, 2011.

[27] Y.Z. Qian and S.E. Woosley. Nucleosynthesis in Neutrino-driven Winds. I. The Physical Conditions. *Astrophys.J.*, 471:331, 1996.

[28] G. Cacciapaglia, M. Cirelli, Y. Lin, and A. Romanino. Bulk neutrinos and core collapse supernovae. *Phys.Rev.*, D67:053001, 2003.

[29] N. Lyons, P.T. O'Brien, B. Zhang, R. Willingale, E. Troja, et al. Can X-Ray Emission Powered by a Spinning-Down Magnetar Explain Some GRB Light Curve Features? *MNRAS*, 409:531–540, dec 2009.

[30] J.M. Lattimer and M. Prakash. Neutron Star Structure and the Equation of State. *Astrophys.J.*, 550:426–442, 2001.

[31] Anatoly Spitkovsky. Time-dependent force-free pulsar magnetospheres: axisymmetric and oblique rotators. *Astrophys.J.*, 648:L51–L54, 2006.

[32] A.I. MacFadyen, S.E. Woosley, and A. Heger. Supernovae, jets, and collapsars. *Astrophys.J.*, 550:410, 2001.

[33] Wei-Qun Zhang, S.E. Woosley, and A. Heger. Fallback and Black Hole Production in Massive Stars. *Astrophys.J.*, 2007.

[34] Y. Lyubarsky and J.G. Kirk. Reconnection in a striped pulsar wind. *Astrophys. J*, 2000.

[35] Lorenzo Sironi and Anatoly Spitkovsky. Relativistic Reconnection: an Efficient Source of Non-Thermal Particles. *Astrophys.J.*, 783:L21, 2014.

[36] Mickal Melzani, Rolf Walder, Doris Folini, Christophe Winisdoerffer, and Jean M. Favre. Relativistic magnetic reconnection in collisionless ion-electron plasmas explored with particle-in-cell simulations. *Astrophys. J*, 2014.

[37] Maxim Lyutikov and Roger D. Blandford. Gamma ray bursts as electromagnetic outflows. *Astrophys. J*, 2003.

[38] C. Thompson. A Model of Gamma-Ray Bursts. *MNRAS*, 270:480, 1994.

[39] E.E. Fenimore and E. Ramirez-Ruiz. The observational basis for central engines in gamma-ray bursts. *Astrophys. J*, 1999.

[40] Phil Evans. Swift XRT-GRB Catalogue. `http://www.swift.ac.uk/xrt_live_cat/`, 2014. [Online].

[41] David W. Hogg, Ivan K. Baldry, Michael R. Blanton, and Daniel J. Eisenstein. The K correction. 2002. [Pedagogical review on arxiv].

[42] Sandra Savaglio. GRB Host Studies. `grbhosts.org`, 2014. [Online].

[43] Ned Wright. CosmoCalc. `http://www.astro.ucla.edu/~wright/CosmoCalc.html`, 2008. [Online].

[44] H. Shen, H. Toki, K. Oyamatsu, and K. Sumiyoshi. Relativistic Equation of State for Core-collapse Supernova Simulations. *Astrophys. J*, 197:20, 2011.

[45] J.D. Kaplan, C.D. Ott, E.P. O'Connor, K. Kiuchi, L. Roberts, et al. The Influence of Thermal Pressure on Hypermassive Neutron Star Merger Remnants. *Astrophys. J*, 2013.